Atomic Spectroscopy

Article

Low-damage Femtosecond Laser-induced Plasma Spectroscopy for Rapid Differentiation of the Surface Hardness of Steel

Lukas Retterath, Peter Kohns, and Georg Ankerhold*

Faculty of Mathematics, Informatics, Technology, University of Applied Sciences Koblenz, Campus Remagen, 53424 Remagen, Germany

Received: *September 24, 2025;* ***Revised:*** *November 04, 2025;* ***Accepted:*** *November 05, 2025;* ***Available online:*** *November 05, 2025.*

DOI: 10.46770/AS.2025.156

ABSTRACT: This proof-of-concept study investigates the application of femtosecond laser-induced breakdown spectroscopy (fs-LIBS) for a rapid, almost non-destructive assessment of surface hardness of 80CrV2 steel samples subjected to thermal treatment. Conventional hardness testing methods, such as Vickers and Rockwell, often necessitate extensive sample preparation, geometric requirements and can alter the material's surface, limiting their effectiveness for rapid assessments. In contrast, LIBS offers a contactless approach that minimizes surface damage while providing high spatial resolution. In previous work, we have already shown that nanosecond laser-induced breakdown spectroscopy (ns-LIBS) leads to melt and material redeposition around craters, consequently reducing the achievable effective spatial resolution. To circumvent these problems, we used femtosecond laser pulses to generate reproducible plasmas on 80CrV2 steel samples with varying degrees of hardness. By maintaining consistent parameters such as laser energy, surface roughness, and planarity, this method facilitates the analysis of spectral changes associated with mechanical properties. Our results identify a correlation between the intensity ratios of iron emission lines and material hardness, underscoring the method's sensitivity to microstructural material changes. As expected, the femtosecond laser-induced breakdown spectroscopy technique (fs-LIBS) produced significantly smaller ablation craters than ns-LIBS. When accounting for the fluence changes resulting from crater formation and making the necessary adjustments, repeated measurements at the same locations could become feasible in the future. A method using fs-LIBS could be a compelling alternative for hardness testing of finely structured or heat-sensitive components.

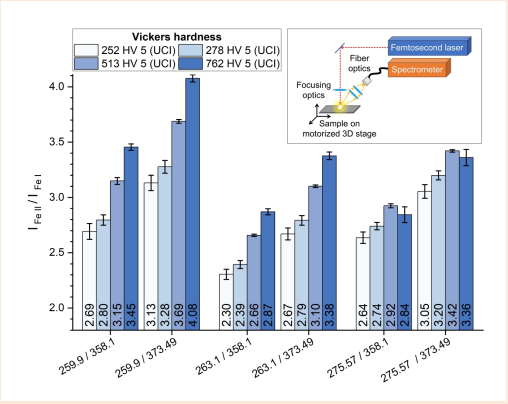

INTRODUCTION

The versatility and adaptability of steel in a variety of applications is characterized by the targeted combination of alloy components and heat treatments.[1] Steel is often heat treated to improve machinability and optimize desired mechanical properties, especially hardness.[2] This is particularly important in applications that require high abrasion resistance, making it crucial to quickly distinguish between soft and hardened steel components to ensure product quality.[1-3]

Common hardness testing methods, such as Brinell, Rockwell, and Vickers, measure indentation sizes caused by mechanical impression.[2, 3] Despite their ubiquity, these tactile methods necessitate time-consuming sample preparation, such as grinding or polishing, are constrained by geometric limitations, and generally result in alterations or damage to the surface.[3] Due to these limitations, these methods are not ideal for rapidly and non-destructively determining component hardness, particularly when high spatial resolution or measurements in mechanically challenging locations are required.[1-4]

Laser-induced breakdown spectroscopy (LIBS) emerges as a promising alternative in this regard. This method facilitates a contactless, almost non-destructive assessment of material properties with minimal preparation effort.[5-11] A contactless laser method is particularly well-suited for quickly distinguishing between areas of components that have been differently hardened through heat treatment, as it generally provides high spatial resolution,[6-9] while the spectral analysis of plasma generated by

short laser pulses provides insights into mechanical properties, such as hardness.[9, 10]

In the field of materials science, LIBS has established itself as a successful and widely adopted method for determining the mechanical properties of materials. Tsuyuki *et al.*[12] were the first to observe a correlation between the intensity ratio of calcium emission lines and the strength of concrete, while Abdel-Salam *et al.*[13] reported similar findings for calcified tissues. In addition to these two pioneering publications, a substantial body of research conducted over the past two decades has revealed a strong correlation between laser-induced plasma properties, such as temperature and the ratio of ionic to atomic line intensities, and the mechanical hardness multiple times and on a wide range of materials, all using nanosecond laser pulses. This includes research on aluminum–lithium alloys and lithium ferrites,[14] bio-ceramics,[15] alumina-based ceramic nanocomposites,[16] α-alumina samples,[17] graphite/rubber composites,[18] lead glass,[19] as well as geological[20] and biological samples.[21]

In addition to these materials, LIBS has also been used in the investigation of metallic alloys to determine or analyze the influence of hardness. This for example has been demonstrated by Khalil et al. for aluminum alloys,[22] Kim *et al.* for welded steel,[23] Messaoud Aberkane *et al.* for iron alloys,[24] Mohamed *et al.* for titanium-based alloys,[25] Sattar *et al.* for tungsten heavy alloys,[26] Momcilovic *et al.* for aluminum alloys and cast iron,[27] and ElFaham *et al.* for spring steel alloys.[28]

In a preceding study, we already demonstrated the potential of LIBS imaging to differentiate between soft and hardened regions of a single carbon steel component.[9] However, we also observed that the use of nanosecond laser pulses with typical pulse energies of several 10 mJ led to significant material melting and redeposition, which impaired the differentiation of hardness differences and made it impossible to take new measurements at the same locations.

The present work, therefore, employs the approach of using femtosecond laser pulses to potentially overcome these drawbacks and to expand the methodology for determining hardness. As detailed by Labutin et al.[29] in their review on femtosecond laser-induced plasma spectroscopy, femtosecond lasers offer significant advantages over nanosecond lasers, obviously primarily consisting of higher peak power and shorter interaction times. These may contribute to enhancements in plasma generation and sensitivity in detecting hardness variations. Furthermore, the minimal surface damage associated with cold ablation and a highly spatially confined heat-affected zone may permit repeated measurements at the same position without significantly altering the specimen's surface, thereby facilitating depth profiling and high-resolution mappings. A more recent work by Galmed et al.[30] demonstrates that fs-LIBS offers a promising approach for the analysis of titanium alloys with varying degrees of hardness, while concurrently mitigating surface damage.

For our own research on fs-LIBS for material hardness evaluation, we obtained steel samples from the same raw material. This allows us to directly assess the effects of heat treatment on hardness without the influence of differences in alloy composition. Given the sensitivity of LIBS methods to variations in surface roughness and planarity, meticulous care was taken to maintain these parameters consistently throughout the experimental process. A sufficiently slow sample movement ensured a stable plasma signal throughout the integration time of the cost-effective, ungated spectrometer used in this study. This approach was chosen based on our own tests, which showed that applying rapid laser pulses to the same position not only resulted in hole drilling but also caused a significant increase in surface roughness, findings consistent with those reported by Wynne and Stuart[31]. Consequently, this leads to an increase in the irradiated surface area and a rapid decrease in laser fluence, lowering the ablation rate and plasma signal strength.

Still, our methodology shares advantages of ns-LIBS over conventional mechanical testing methods, including being contactless and nearly non-destructive by avoiding surface deformation and enabling measurements with high spatial resolution, with the effective spatial resolution possibly benefiting even more from the minimal heat-affected zone of fs-LIBS.

Prior to the analysis of material hardness via spectral methods, a comparative investigation was conducted on the effects of femtosecond and nanosecond laser pulses on the surface structure of the samples. The short interaction time of femtosecond lasers ensures minimal heat transfer to surrounding material, which prevents the formation of molten droplets and deposits. This capability could possibly allow for repeated measurements at the same locations, which would be particularly advantageous for industrial applications. It could help minimize outliers in the measurement results by enabling averaging over multiple pulses.

Following the examination of potential surface alterations and signal stability, we used the same two distinctly different hard steel surfaces to assess possible plasma emission changes. Finally, our investigations concluded with measurements of several intensity ratios of ionic to atomic emission lines of iron taken on various regions of a steel piece with a hardness gradient along its longitudinal axis.

EXPERIMENTAL

Setup. Fig. 1 shows a schematic illustration of the experimental setup. It consists of a commercial femtosecond pulse laser (NKT

Table 1. Chemical composition of the low-alloy carbon spring steel DIN 80CrV2 in wt%.[32]

Symbol DIN	C (%)	Si (%)	Mn (%)	P (≤ %)	S (≤ %)	Cr (%)	Mo (≤ %)	Ni (≤ %)	V (%)	Cu (%)
80CrV2	0.75 -0.85	0.15 -0.35	0.30 -0.50	0.025	0.025	0.40 - 0.60	0.10	0.40	0.15 -0.25	0.40

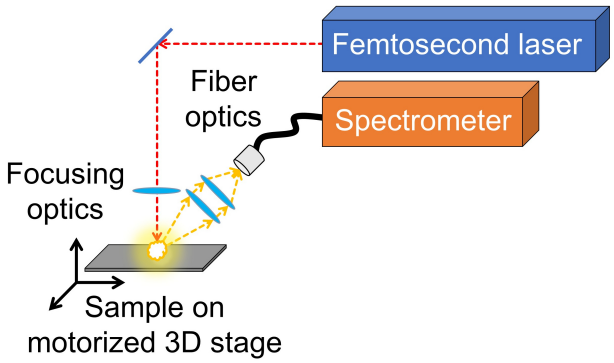

Fig. 1 Schematic illustration of the experimental setup, featuring a femtosecond laser and an ungated spectrometer.

Photonics ORIGAMI 10 XPS) that emits laser pulses (1030 nm, 315 fs) with pulse energies of up to 70 µJ at a repetition rate of 50 kHz. These pulses are focused on the sample surface within a spot with a calculated diameter of 30 µm. At the primarily used setting of 30 µJ, this results in a laser fluence of about 4.24 J/cm² and a peak power density of nearly 13.5 TW/cm². Following manual focus adjustment, the flat steel pieces are subsequently moved beneath the laser beam at a constant speed of approximately 3.5 millimeters per second by means of a computer-controlled 3D stage (Lasertechnik Berlin).

Plasma was obtained in ambient air at standard atmospheric pressure and room temperature. Its emission was collected at a 45-degree angle to the sample surface and the laser beam, respectively, by two 1-inch plano-convex fused silica lenses (ThorLabs LA4148, focal length 50 mm). Spectral detection was achieved using an optical multimode fiber with a core diameter of 400 µm, which was connected to a USB spectrometer (OceanOptics Maya2000 Pro). Its spectral range covers 190 to 416 nm with a sensor resolution of approximately 130 pm, which is well-suited to the detection of Fe emission lines. Integration times were set to the minimum possible value of 10 milliseconds, with the sample moving beneath the laser pulses to achieve reliable plasma signal. Each sample or region for measurements on the long piece underwent six scans, during which the spectra for each scan line were recorded. This process resulted in the acquisition of approximately 100 spectra for each line scan. Acquisition was started while the samples were already moving under the pulsed laser beam. Thus, a consistent moving speed without any acceleration could be achieved.

The preprocessing of data was conducted prior to the measurement of line intensity ratios and consisted of the subtraction of background and subsequential averaging of the spectra of each scan line. The resulting six background subtracted and averaged line spectra were used to assess hardness-dependent variations in emission. Due to the ungated spectral detection of the full plasma lifespan from 500 laser pulses per integration interval, a prominent broad background was expected. It was not corrected to circumvent any potential alteration of the spectral information.

Samples. DIN 80CrV2 steel was acquired from Schmiedeglut GmbH in the form of a long bar with a thickness of 5 mm and a width of 40 mm. It was then cut into smaller pieces, two measuring approximately 20 mm for initial investigations into the impact of surface hardness on the resulting spectra and SEM analyses of laser pulse surface alterations, and another piece measuring about 130 mm in length for our intensity ratio measurements. Classified as a low-alloy steel, its constituent elements collectively account for less than 5 mass percent, as indicated by the low concentrations of alloying elements presented in Table 1.[32] This steel is commonly used in the manufacturing of knives and cutting blades.

To achieve varying levels of material hardness, one of the smaller pieces was left untreated and remained in its original soft state. The other single piece and the long piece were placed in a muffle furnace (Nabertherm L15/13) and gradually heated at a temperature rate of 350 K/h to the target soaking temperature of 830 °C.[33] Considering the dimensional parameters, the individual soaking times were calculated to a minimum of 30 min for the small piece and 50 minutes for the long steel piece.[34] After soaking, the hot single steel piece underwent rapid cooling (quenching) in 18 °C cold water, resulting in a rapid cooling rate that induced a phase transformation and modification of the lattice structure in the material. It is well known that martensitic transformation is the primary cause of the hardness observed in quenched steel.[2, 4] For the long piece, one end of the hot sample was submerged about 50 mm deep into 18 °C cold water. This resulted in a hardness gradient along the longitudinal axis, as described in more detail in previous work.[9] Due to the high brittleness of quenched steel, an additional tempering step is commonly necessary to relieve internal stress while preserving the majority of its hardness. The two small pieces were tempered twice at 150 °C for 1 h per cycle.

The application of the heat treatment process resulted in the production of both hardened and soft steel pieces, as well as an additional piece exhibiting varying hardness across its surface. To investigate the influence of varying surface hardness on our LIBS measurements, we used the two distinctively different hard samples and selected four regions on the longer sample that

encompassed not only the two extremes, the soft end and the fully quenched hard end, but also intermediate hardness range. One region was located just above the immersion water level during quenching, while another was positioned between the softest region and the previously mentioned section.

To assess the hardness of the regions of interest, Vickers hardness tests (INNOVATEST NEXUS 7700) and the Ultrasonic Contact Impedance method (UCI, SaluTron HardyTest UCI3000) were employed.[35,36] Hardness values were measured at 221 ± 11.5 HV 0.5 (Vickers) and 224 ± 15 HV 5 (UCI) for the single soft piece, and 761 ± 17.1 HV 0.5 (Vickers) and 780 ± 20 HV 5 (UCI) for the single hardened piece, respectively. The hardness of the inspected regions on the partially hardened longer steel piece was measured at 252 ± 15 HV 5 (UCI), 278 ± 15 HV 5 (UCI), 513 ± 20 HV 5 (UCI), and 762 ± 20 HV 5 (UCI). The given error values represent the standard deviation of our Vickers hardness tests, and the expected measurement accuracy for the UCI method, as specified by the device manufacturer. To ensure uniform roughness and planarity, all samples were meticulously wet-ground using a resin-bonded diamond grinding disk (finish comparable to FEPA P120). For scanning electron microscope investigations, an additional polishing step was performed using a polishing cloth disk and a suitable diamond solution (3 µm grain size).

RESULTS AND DISCUSSION

As already noted, the physical interaction of femtosecond laser pulses with the material surface fundamentally differs from that of longer pulses, leading to a significant reduction in thermal damage and the heat-affected zone.[29,37,38] This characteristic could also be a key advantage for spatially resolved measurements as shown by Wessel *et al.*[8] To investigate this aspect, we employed scanning electron microscopy (SEM, TESCAN Vega 4) to analyze the crater morphology following laser irradiation, as illustrated in Fig. 2. The results revealed distinct differences between craters formed by nanosecond (Fig. 2a) and femtosecond (Fig. 2b) pulses. Craters formed by nanosecond pulses generally display redeposition of molten material surrounding the crater, while femtosecond pulse craters are characterized by their smoother edges, a consequence of the minimal heat-affected zone and thus impact on adjacent material. This advantage enables measurement points to be placed in close proximity, an issue we identified as a major limitation of ns-LIBS.[9]

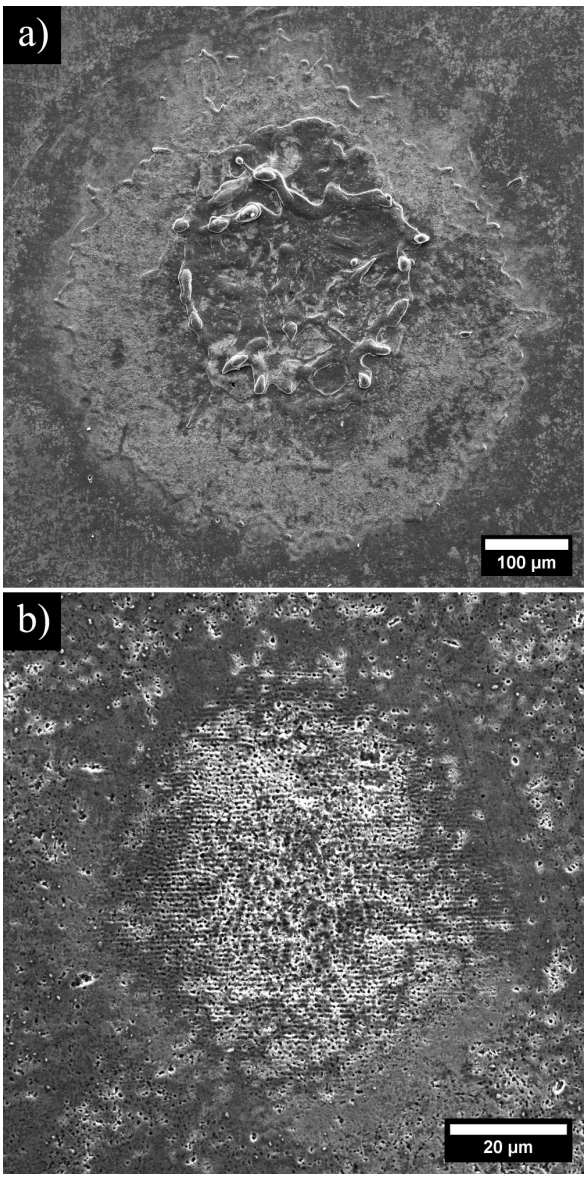

Fig. 2 Comparison of crater sizes and the surrounding affected areas when applying (a) a single nanosecond laser pulse (4 ns, 75 mJ) and (b) ten consecutive femtosecond laser pulses (315 fs, 30 µJ per pulse) on hardened steel (780 ± 20 HV 5 (UCI)). The area affected by (a) the nanosecond crater, including melt deposition, is several times larger than the 68 µm laser spot size and spans approximately 600 µm in diameter. In contrast, (b) the femtosecond crater, free of significant melt deposits, is confined to approximately 65 µm in diameter, about twice the optimal focus spot size of 30 µm.

However, when applying multiple femtosecond laser pulses to identical positions, the resulting crater morphology must also be considered. Preceding tests on the evolution of signal strength when ablating single spots with a high-repetition-rate laser confirmed the findings of Wynne and Stuart[31]. Using a fast photodiode and suitable spectral filters we observed a significant decrease in the plasma signal after 10 to 20 femtosecond laser pulses without sample movement. The signal decreased to about one-third of that created by the first pulse and became not any longer detectable with our ungated spectrometer after 1 millisecond. Given the laser repetition rate of 50 kHz, this means that the decrease occurs in less than one-tenth of the minimal integration time of our ungated spectrometer (10 ms). Further investigations into crater morphology after higher numbers of

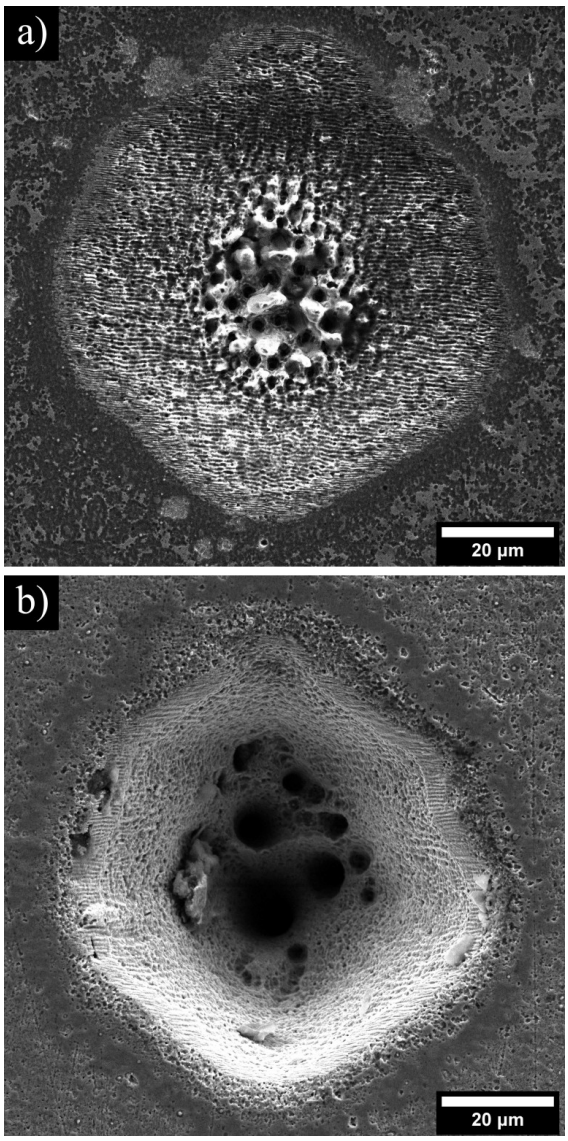

Fig. 3 Comparison of crater sizes and morphology when applying (a) 100 and (b) 1000 subsequent femtosecond pulses (315 fs, 30 µJ per pulse) on hardened steel (780 ± 20 HV 5 (UCI)).

laser pulses reinforce these findings on plasma signal evolution. Fig. 3 shows two additional SEM images of craters produced by 100 (Fig. 3a) and 1000 femtosecond laser pulses (Fig. 3b), each with an energy of 30 µJ. A comparison with the crater displayed in Fig. 2b reveals a substantial increase in both crater depth and surface roughness. This is likely to cause a significant reduction in the achievable effective laser fluence, thereby affecting the levels of ablation and plasma signal. Nonetheless, when looking at the SEM images, the advantage of spatially confined ablation remains evident, as the diameters of all craters (Fig. 2b, Fig. 3a, Fig. 3b) are approximately consistent across all three conditions, highlighting the core benefits of femtosecond ablation.

The findings related to crater morphology and signal stability are the reason for the methodology employed in this study. The approach, involving constant sample movement under the pulsed laser, ensures a consistent material feed for plasma generation. Given the low scan speed of approximately 3.5 mm per second and the laser pulse repetition rate of 50 kHz, the occurrence of overlapping laser craters during testing was obvious, as the sample moved only 70 nm between two successive laser pulses. In relation to the methodology, we tested the impact of pulse energy on the resulting scan lines while moving at specified speed. The detailed scan images in Figs. 4a and 4b illustrate the influence on (a) soft surface (hardness: 224 HV 5 (UCI)) and (b) a hardened surface (hardness: 780 HV 5 (UCI)). The borders are quite similar for lines generated with pulse energies of 10 µJ, 30 µJ, 50 µJ, and 70 µJ, respectively. Only the line depth varies slighty with different laser energy settings. Significant differences in surface modifications between soft and hard materials are not apparent, as the lines are only slightly wider than the laser spot size of approximately 30 µm for both steel hardness values. This, in addition to the spatially confined craters in Fig. 3, further demonstrates that femtosecond laser-induced breakdown spectroscopy could be highly beneficial for ongoing research involving spatially resolved investigations. Our tests indicated that a pulse energy setting of 30 µJ represented the optimal compromise for achieving stable and reliable emission with minimal surface alteration. This means that with the stage speed set to approximately 3.5 mm per second, each focal spot was irradiated by roughly 430 laser pulses, resulting in an average fluence of around 1.8 kJ/cm².

To investigate the spectral influence of differently hardened steel surfaces, plasmas were generated using femtosecond laser pulses at a repetition rate of 50 kHz. The previously described samples were positioned on a digitally controlled translation stage and moved at a constant speed under the laser beam. As noted, this uniform movement was crucial for maintaining a constant supply of material, allowing the resulting plasma plume to be emitted continuously and with adequate intensity. Given the high sensitivity to variations in laser energy, overall surface roughness, and sample flatness in relation to the incident laser beam, we have taken great care to control these parameters and ensure consistency throughout the process.

Plasmas induced by femtosecond pulses have significantly shorter lifetimes than those generated by nanosecond pulses. Their lifetimes typically range from a few hundred nanoseconds to even shorter durations, making them challenging to detect.[39] Reliable acquisition of single laser-induced plasma plumes would necessitate sophisticated, high-speed, and precisely gated measurements and readout electronics. Therefore, a compromise was established to on the one hand minimize sample damage while on the other hand still producing a sufficiently intense emission. It was deemed reasonable to accumulate the emission from multiple pulses using an ungated spectrometer to generate a

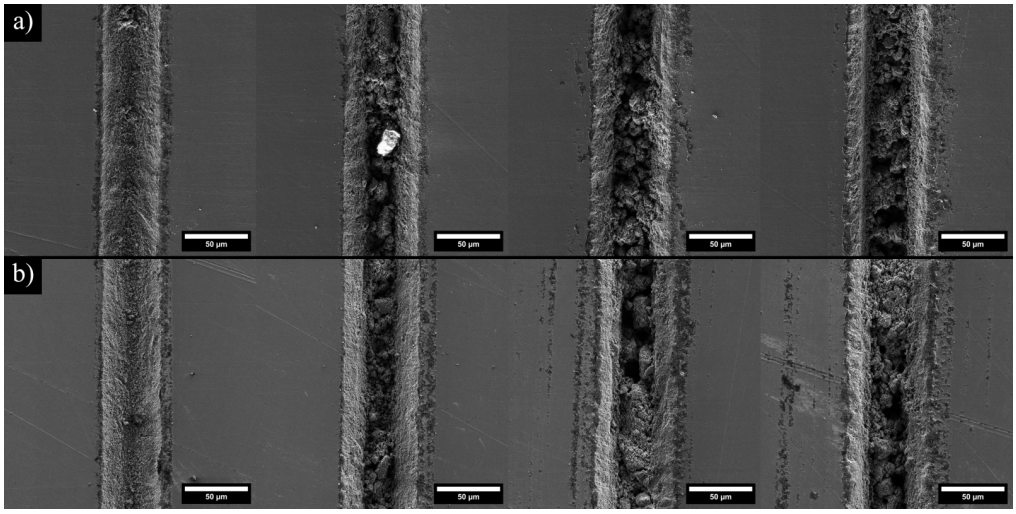

Fig. 4 Surface alterations induced by scanning at 3.5 mm/s using femtosecond laser pulses (315 fs, 50 kHz) on steel with varying hardness at energy levels of 10 µJ, 30 µJ, 50 µJ, and 70 µJ (left to right); (a) soft sample (hardness: 224 HV 5 (UCI)), (b) hardened sample (hardness: 780 HV 5 (UCI)).

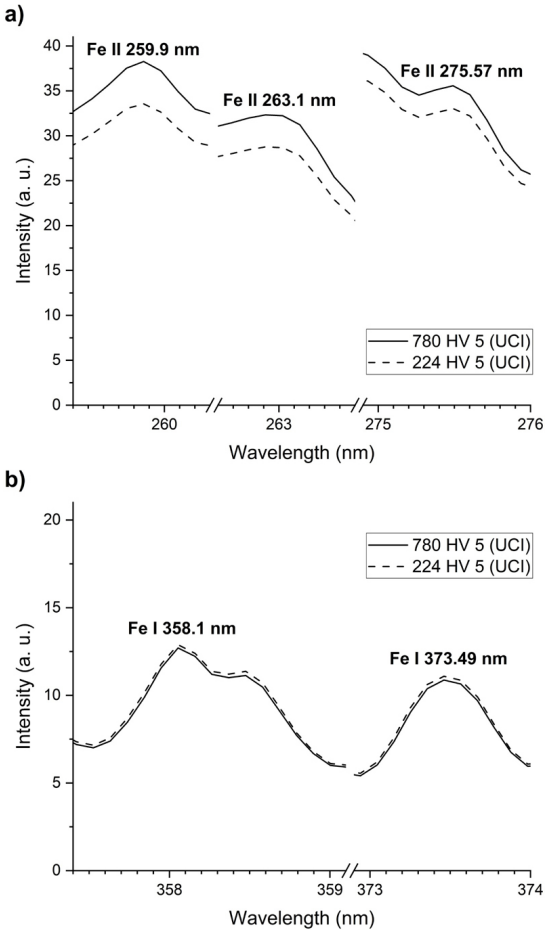

Fig. 5 Surface hardness-related intensity changes for (a) ionic and (b) atomic emission lines of iron on soft (224 HV5 (UCI)) and hardened (780 HV5 (UCI)) 80CrV2 samples. Hardness was determined using the Ultrasonic Contact Impedance (UCI) method.[36]

still representative spectrum. The set integration time of 10 ms corresponds to approximately 500 laser pulses per spectrum at a repetition rate of 50 kHz, which we found to allow for reliable capture of the emission. As previously mentioned and demonstrated by investigating the impact of pulse energy on surface alteration (Fig. 4), the optimal pulse energy setting was determined through a balanced approach that considered both the reduction of surface damage and the maintenance of a robust signal.

Impact of surface structure, including roughness and flatness, which must be considered when focusing on a spot of only a few tens of micrometers, was also reduced by the chosen approach. Despite these considerations, particular care was taken to maintain consistent measurement parameters, ensuring that observed spectral variations could be primarily attributed to differences in the surface hardness of the steel samples.

To thoroughly evaluate the fundamental functionality of our novel hardness determination approach using fs-LIBS and to investigate possible spectral changes, we initially focused on the single soft sample and the single hardened sample. Fig. 5 shows several characteristic iron emission lines in the spectra of plasmas generated on these two samples with distinctively different levels of hardness. While the spectral emissions are similar due to the identical alloy components, noticeable differences in signal maxima and variations in the intensities of iron ionic (Fig. 5a) and atomic emission lines (Fig. 5b) are evident.

These findings support the results and conclusions of our preceding work, which explored an approach using nanosecond pulses and single-shot measurements, and also reported on changes in the ratio of ionic to atomic line intensities of iron.[9] They

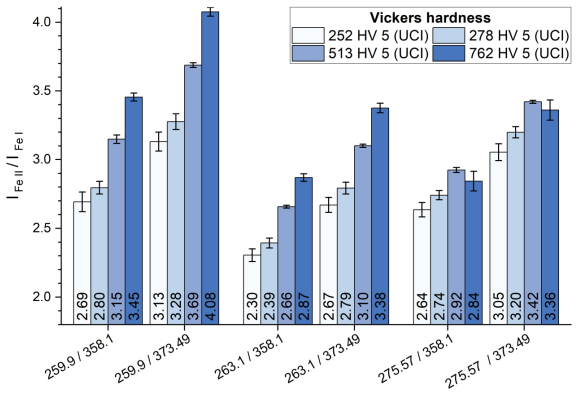

Fig. 6 Intensity ratios for several line pairs (ionic and atomic) in different hard areas of a partially hardened steel piece. The error bars represent the standard deviation from the six scans conducted per hardness region.

further indicate that variations in bonding strength and lattice configuration within the material influence ablation efficiency, even when considering different pulse-material interaction mechanisms associated with shorter pulse widths. A direct correlation between material hardness and ablation volume is documented for nanosecond laser ablation.[14] But unlike nanosecond ablation, where the plasma plume forms during the pulse and experiences additional heating from the trailing parts of the pulse, femtosecond laser-generated plasmas do not exhibit laser-plasma interaction. This is due to the pulse duration being shorter than the characteristic energy relaxation times on the picosecond timescale where the absorbed energy transfers to the lattice due to electron-phonon coupling. Consequently, this results in an after-pulse phase explosion, where electrons emitted from the surface create an electrostatic field that pulls ions out of the surface.[29, 40, 41] This means that the complete deposition of photon energy into the material occurs through inverse Bremsstrahlung before any electron-lattice heating or plasma formation can take place.[37, 38]

To validate our concept on distinguishing surface hardness by measuring the intensity ratios between ionic and atomic emission lines of iron, we extended our measurements to a sample with regions of varying hardness. The results of our investigations are presented in Fig. 6, where the column chart displays the measured intensity ratios of selected iron emission lines. The x-axis labels indicate the wavelength, in nanometers, of the ionic and atomic emission lines of iron used for measuring the ratio. For example, "259.9 / 358.1" represents the measured ratio value of $I_{\text{Fe II 259.9 nm}}$ to $I_{\text{Fe I 358.1 nm}}$. A distinct increase in these ionic to atomic intensity ratios can be observed when transitioning from softer to harder surface regions with the trend being consistent across various emission line ratios. The depicted ratio values represent the average across all six individual scans per sample with the error bars representing the resulting standard deviation between the scans. Notably, only the measured ratios using the ionic emission line at 257.57 nm exhibit a decreased average value for the region with the highest surface hardness. But the higher standard deviation compared to those achieved on the other surface areas suggests that it may still be possible to differentiate hardness if this variability is taken into account.

Figure 7 illustrates a graph that establishes a quantitative relationship between mechanically measured hardness and intensity ratio values. The data points represent the average across six individual scans per sample, with the y-axis error bars indicating the resulting standard deviation. The error bars on the x-axis reflect the expected measurement accuracy for the UCI method, as specified by the device manufacturer. We excluded the ratios derived from the ionic emission line at 257.75 nm due to the noted decrease in ratio for the hardest sample region. The remaining intensity ratios show a strong positive linear correlation with hardness, as indicated by the high regression coefficients. However, it is important to note that we cannot definitively exclude the possibility of other correlations. The results also highlight the crucial role of selecting suitable emission lines and underscores the need for further extensive research to develop a robust model. Additionally, it is important to note that our tests were conducted using only a single steel alloy; hence, the present work should be regarded as a proof of concept, requiring additional investigations for successful industrial implementation.

CONCLUSION

In this study, we explored the application of femtosecond laser-induced breakdown spectroscopy (fs-LIBS) for evaluating surface hardness of DIN 80CrV2 steel. To create a sample with a hardness gradient and minimize variations in chemical composition, we subjected a single piece of steel to heat treatment, followed by partial quenching. For the effective implementation of our contactless hardness differentiation method using fs-LIBS, several critical factors had to be considered. These included maintaining constant laser parameters and ensuring consistent surface properties, such roughness and planarity of the sample relative to the incident laser beam.

The results of this proof-of-concept work demonstrated that fs-LIBS, when combined with continuous sample movement, effectively generated reproducible plasmas with stable emission signals while minimizing thermal damage. The observed correlation between intensity ratios of selected iron emission lines and mechanical hardness indicated that microstructural changes affect the ablation process and the resulting plasma emission. We summarize our physical explanation for the observed effect as follows. Unlike the hardness-dependent material ablation volume, which is further heated by trailing parts of a nanosecond pulse, thereby increasing ionization, the use of femtosecond laser pulses enables spectral differences to be attributed to variations in the

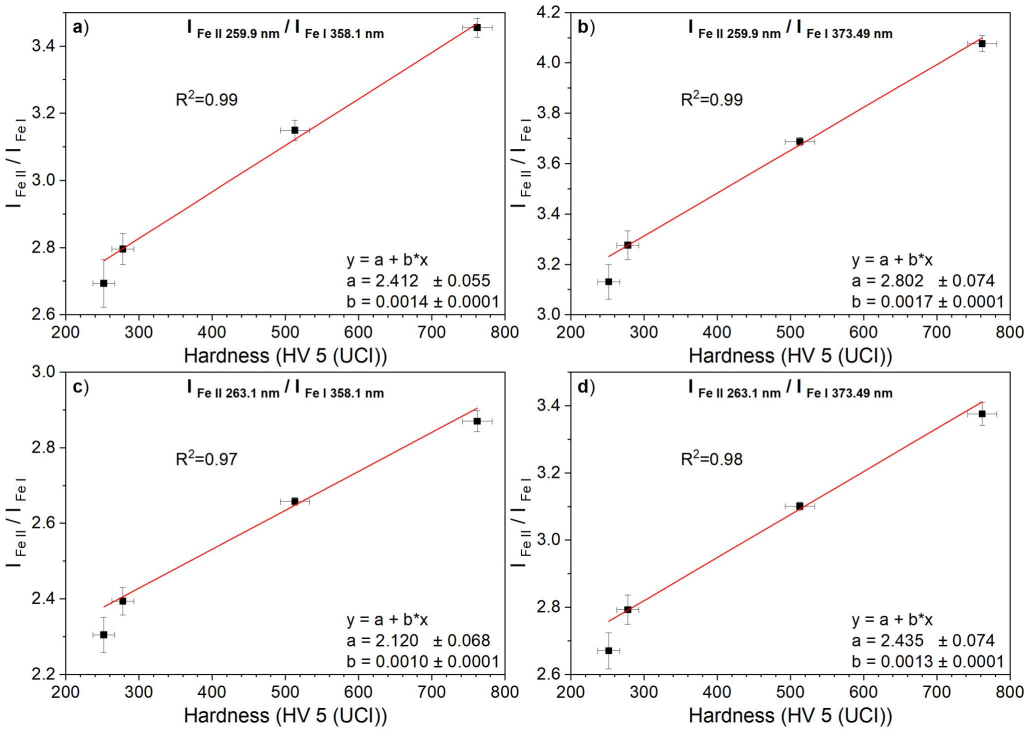

Fig. 7 Strong positive linear correlation, as indicated by the high regression coefficients, between different line intensity ratios ($I_{Fe\,II} / I_{Fe\,I}$) and mechanically determined material hardness, with the x-axis error bars representing the expected measurement accuracy for the UCI method, as specified by the device manufacturer, and y-axis error bars indicating the resulting standard deviation. The equations for each linear fit are shown in the bottom right corner of each graph (a-d).

microstructure of the material itself. These variations may directly influence photon energy absorption and the subsequent redistribution of the absorbed energy to the lattice and ions.

The presented method allowed for the differentiation of hardness while simultaneously reducing surface alteration. Our findings further indicate that fs-LIBS could be a particularly promising alternative for achieving spatially precise and minimally destructive hardness differentiation, as it results in a minimal heat-affected zone and produces smaller craters that are nearly free from thermally induced edge damage, potentially providing significant advantages for finely structured, heat-sensitive or brittle components.

Overall, it is evident that both conventional laser-induced breakdown spectroscopy using nanosecond pulses and fast gated spectrometers, as well as the proof-of-concept presented in this study employing femtosecond pulses, constant material feed by sample movement and extended integration times, could offer unique advantages when compared to conventional methods. Insights gained from this research highlight the potential of fs-LIBS as a valuable tool for material characterization in both research and industrial contexts. It is important to emphasize that this study focused solely on one specific type of steel alloy, 80CrV2, and is therefore only applicable to low-alloy steels. Since chemical composition significantly influences heating dynamics and plasma evolution, future investigations should expand this methodology to include additional steel alloys and various intermediate hardness states. Combining this approach with imaging techniques and time-resolved spectroscopy could enhance our understanding of the complex plasma-material interactions. Exploring other materials that could benefit from the minimal heat-affected zone, or where conventional mechanical hardness measurements pose challenges, such as ceramics, time-dependent hardening process of concrete, rubbers, and other composites, may also be of considerable industrial interest.

AUTHOR INFORMATION

Lukas Retterath earned his BSc in Optics and Laser Technologies in 2020 and his MSc in Applied Physics in 2023 from the University of Applied Sciences Koblenz, Germany. Currently, he is a doctoral student in the Faculty of Mathematics, Informatics, Technology at the same institution, primarily focusing on laser-induced breakdown

spectroscopy, a technique he has been actively studying since his undergraduate years. His research also encompasses several related fields, including atomic and molecular spectroscopy, laser material processing, and microscopy.

Peter Kohns received his Diploma in Physics in 1989 and his doctorate in 1993 from the University of Bonn, Germany. He has served as the head of development for two companies and is currently a Professor in the Faculty of Mathematics, Informatics, Technology at the University of Applied Sciences Koblenz, Germany. His work covers various topics, including laser-induced breakdown spectroscopy, laser material processing, and optical design. Since 1994, he has been working with femtosecond lasers.

Georg Ankerhold received his Diploma in Physics from Leibniz University Hannover in 1987 and earned his doctorate in Physics from the University of Münster, Germany, in 1993. He subsequently held senior industry positions in optical sensor technology, optical spectroscopy, and laser lithography development. He is currently Professor of Physics and Dean of the Faculty of Mathematics, Informatics, Technology at the University of Applied Sciences Koblenz. His research work focuses on atomic and molecular spectroscopy, in particular laser-induced breakdown spectroscopy, Raman spectroscopy, and optical sensor technologies. Since 2015, he has also been working with femtosecond pulse lasers and their interaction with matter. He has published more than 70 papers and holds 14 patents.

Corresponding Author

*G. Ankerhold

Email address: ankerhold@hs-koblenz.de

Notes

The authors declare no competing financial interest.

ACKNOWLEDGMENTS

The authors gratefully thank Robert Pandorf and Benjamin Dünnes from the Faculty of Engineering at the University of Applied Sciences Koblenz for their valuable expertise and support with steel-related inquiries and tactile measurements of our samples in the Materials Science Laboratory at Campus Koblenz, Germany. Additionally, the authors thank Andreas Haidl from the Faculty of Mathematics, Informatics, Technology at the University of Applied Sciences Koblenz for his technical assistance in operating the scanning electron microscope at Campus Remagen, Germany.

REFERENCES

1. W. Weißbach and M. Dahms, Werkstoffkunde: Strukturen, Eigenschaften, Prüfung. Springer Fachmedien Wiesbaden, 2015. https://doi.org/10.1007/978-3-658-03919-6
2. H. J. Bargel, Werkstoffkunde: Strukturen - grundlegende Eigenschaften. Springer Berlin Heidelberg, 2022. https://doi.org/10.1007/978-3-662-63961-0
3. A. Bhaduri, Mechanical properties and working of metals and alloys. Springer Singapore, 2018. https://doi.org/10.1007/978-981-10-7209-3
4. W. D. Callister Jr and D. G. Rethwisch, Materials science and engineering: an introduction. John Wiley & Sons, 2020. http://wiley.com/go/Callister_MaterialsScienceGE
5. R. Noll, Laser-Induced Breakdown Spectroscopy: Fundamentals and Applications. Springer Berlin, Heidelberg, 2012. https://doi.org/10.1007/978-3-642-20668-9
6. T. Dietz, C. Gottlieb, P. Kohns, and G. Ankerhold, *Spectrochim. Acta B*, 2019, **161**, 105707. https://doi.org/10.1016/j.sab.2019.105707
7. C. Beresko, P. Kohns, and G. Ankerhold, *Spectrochim. Acta B*, 2014, **99**, 20-27. https://doi.org/10.1016/j.sab.2014.06.004
8. W. Wessel, A. Brueckner-Foit, J. Mildner, L. Englert, L. Haag, A. Horn, M. Wollenhaupt, and T. Baumert, *Eng. Fract. Mech.*, 2010, **77**, 1874-1883. https://doi.org/10.1016/j.engfracmech.2010.03.020
9. L. Retterath, P. Kohns, and G. Ankerhold, *Spectrochim. Acta B*, 2024, **219**, 107003. https://doi.org/10.1016/j.sab.2024.107003
10. N. Yang, M. Shan, G. Shi, H. Guo, S. Xiong, M. Luo, D. Zhang, and M. Cui, *Atom. Spectrosc.*, 2024, **45**, 324-335. http://dx.doi.org/10.46770/AS.2024.158
11. J. Cai, M. Dong, Y. Zhang, Y. Chen, H. Chen, Y. Liang, W. Li, and J. Lu, *Atom. Spectrosc.*, 2021, **42**, 43-50. http://dx.doi.org/10.46770/AS.2020.217
12. K. Tsuyuki, S. Miura, N. Idris, K. H. Kurniawan, T. J. Lie, and K. Kagawa, *Appl. Spectrosc.*, 2006, **60**, 61-64. https://doi.org/10.1366/000370206775382668
13. Z. A. Abdel-Salam, A. H. Galmed, E. Tognoni, and M. A. Harith, *Spectrochim. Acta B*, 2007, **62**, 1343-1347. https://doi.org/10.1016/j.sab.2007.10.033
14. T. A. Labutin, A. M. Popov, V. N. Lednev, and N. B. Zorov, *Spectrochim. Acta B*, 2009, **64**, 938-949. https://doi.org/10.1016/j.sab.2009.07.033
15. J. S. Cowpe, R.D. Moorehead, D. Moser, J. S. Astin, S. Karthikeyan, S. H. Kilcoyne, G. Crofts, and R. D. Pilkington, *Spectrochim. Acta B*, 2011, **66**, 290-294. https://doi.org/10.1016/j.sab.2011.03.007
16. K. Ahmad, M. A. Al-Eshaik, and A. N. Kadachi, *Appl. Phys. A*, 2015, **119**, 1223-1229. https://doi.org/10.1007/s00339-015-9167-3
17. K. Yahiaoui, S. Messaoud Aberkane, and A. Naitbouda, *Mater. Chem. Phys.*, 2021, **259**, 124045. https://doi.org/10.1016/j.matchemphys.2020.124045
18. M. M. ElFaham, A. M. Alnozahy, and A. Ashmawy, *Mater. Chem. Phys.*, 2018, **207**, 30-35. https://doi.org/10.1016/j.matchemphys.2017.12.036

19. M. Momcilovic, S. Zivkovic, J. Petrovic, I. Cvijovic-Alagic, and J. Ciganovic, *Appl. Phys. B*, 2019, **125**, 222. https://doi.org/10.1007/s00340-019-7329-2
20. S. N. Panya panya, A. H. Galmed, M. Maaza, B. M. Mothudi, and M. A. Harith, *Mater. Today: Proc.*, 2021, **36**, 600-603. https://doi.org/10.1016/j.matpr.2020.05.766
21. S. S. Dakhil and T. K. Hamad, *Iraqi J. Sci.*, 2024, **65**, 5046-5054. https://doi.org/10.24996/ijs.2024.65.9.21
22. O. M. Khalil, I. Mingareev, T. Bonhoff, A. F. El-Sherif, M. C. Richardson, and M. A. Harith, *Opt. Eng.*, 2014, **53**, 014106. https://doi.org/10.1117/1.OE.53.1.014106
23. J. Kim and C. Ko, *J. Korean Soc. Precis. Eng.*, 2014, **31**, 141-148. https://doi.org/10.7736/kspe.2014.31.2.141
24. S. Messaoud Aberkane, A. Bendib, K. Yahiaoui, S. Abdelli-Messaci, S. E. Amara, and M. A. Harith, *Spectrochim. Acta B*, 2015, **113**, 147-151. https://doi.org/10.1016/j.sab.2015.09.012
25. D. F. Mohamed, A. H. Galmed, and O. A. Nassef, Arab Journal of Nuclear Sciences and Applications, 2017, **50**, 142-155.
26. H. Sattar, H. Ran, W. Ding, M. Imran, M. Amir, and H. Ding, *Appl. Phys. B*, 2020, **126**, 5. https://doi.org/10.1007/s00340-019-7355-0
27. M. Momcilovic, J. Petrovic, J. Ciganovic, I. Cvijovic-Alagic, F. Koldzic, and S. Zivkovic, *Plasma Chem. Plasma Process.*, 2020, **40**, 499-510. https://doi.org/10.1007/s11090-020-10063-5
28. M. M. ElFaham, W. M. Elthalabawy, O. Elzahed, M. A. Zakaria, and M. Abdelhamid, *Appl. Phys. A Mater. Sci. Process.*, 2020, **126**, article number 167. https://doi.org/10.1007/s00339-020-3348-4
29. T. A. Labutin, V. N. Lednev, A. A. Ilyinc, and A. M. Popova, *J. Anal. At. Spectrom.*, 2016, **31**, 90-118. https://doi.org/10.1039/C5JA00301F
30. A. H. Galmed, O. Balachninaite, and O. Aied Nassef, *Opt. Laser Technol.*, 2023, **161**, 109184. https://doi.org/10.1016/j.optlastec.2023.109184
31. A. E. Wynne and B. C. Stuart, *Appl. Phys. A*, 2003, **76**, 373-378. https://doi.org/10.1007/s00339-002-1823-8
32. DIN EN 10132:2022-04, Cold rolled narrow steel strip for heat treatment - Technical delivery conditions; German version EN 10132:2021, (2022). https://dx.doi.org/10.31030/3334919
33. M. Wegst and C. Wegst, Stahlschlüssel Taschenbuch: Wissenswertes über Stähle. Verlag Stahlschlüssel Wegst GmbH, 2007. ISBN-13: 978-3922599227
34. H. Ruhfus, Wärmebehandlung der Eisenwerkstoffe. Verlag Stahleisen, 1958. https://www.deutsche-digitale-bibliothek.de/item/6W4CET2HJDFSUNTC44JCH3QX37QLHTDI
35. DIN EN ISO 6507-1:2024-01, Metallic materials – Vickers hardness test – Part 1: Test method (ISO 6507-1:2023); German version EN ISO 6507-1:2023, (2024). https://dx.doi.org/10.31030/3503781
36. DIN 50159-1:2022-06, Metallic materials - Hardness testing with the UCI method - Part 1: Test method, (2022). https://dx.doi.org/10.31030/3346612
37. B. N. Chichkov, C. Momma, S. Nolte, F. von Alvensleben, and A. Tünnermann, *Appl. Phys. A*, 1996, **63**, 109-115. https://doi.org/10.1007/BF01567637
38. S. S. Harilal, J. R. Freeman, P. K. Diwakar, and A. Hassanein, "Femtosecond laser ablation: Fundamentals and applications." Laser-Induced Breakdown Spectroscopy: Theory and Applications. Berlin, Heidelberg: Springer Berlin Heidelberg, 2014. https://link.springer.com/book/10.1007/978-3-642-45085-3
39. V. Zorba, X. Mao, and R. E. Russo, *Spectrochim. Acta B*, 2015, **113**, 37-42. https://doi.org/10.1016/j.sab.2015.08.011
40. J. König, S. Nolte, and A. Tünnermann, Optics Express, 2005, **13**, 10597-10607. https://doi.org/10.1364/OPEX.13.010597
41. J. Winter, M. Spellauge, J. Hermann, C. Eulenkamp, H. P. Huber, M. Schmidt, Optics Express, 2021, **29**, 14561-14581. https://doi.org/10.1364/OE.421097